ACS OMEGA

Open Access

http://pubs.acs.org/journal/acsodf

Article

Structure and Optical Properties of Sn-Based Halide Perovskites $(C_{10}H_{18}N_2)SnX_4$ (X = Cl, Br, I)

Ruonan Yao, Jiawei Lin,* Kunjie Liu, Yuanchang Xu, Boyi Xiao, Jing Zhao, Zhongnan Guo,* Quanlin Liu, and Wenxia Yuan

Cite This: *ACS Omega* 2024, 9, 22352−22359

Read Online

ACCESS | Metrics & More | Article Recommendations | Supporting Information

ABSTRACT: Low-dimensional tin-based halide perovskites are considered as eco-friendly substitutions of the iconic lead-based perovskites to host the potential as optoelectronic materials. However, a fundamental understanding of the structure−property relationship of these Sn(II)-based hybrids is still inadequate due to the limited members of this material family. To our knowledge, there is still lack of reports on a series of Sn(II)-based halide perovskites with the same organic cation but covering chloride, bromide, and iodide. In this work, three new halide perovskites $TMPDASnX_4$ (X = Cl, Br, I) (TMPDA = N,N,N′,N′-tetramethyl-1,4-phenylenediamine) are successfully synthesized, which provide the ideal paradigm to study the halogen-dependent evolution of the structure and properties of Sn(II)-based hybrid perovskites. Despite sharing the same monoclinic lattice ($P2_1/m$ space group), it is demonstrated that $TMPDASnCl_4$ adopts a one-dimensional structure composed of a five-coordinated pyramid configuration due to an extremely long Sn···Cl distance, while the typical two-dimensional motif is still maintained in $TMPDASnBr_4$ and $TMPDASnI_4$. The ambient stability is declined in the order from chloride to bromide and then to iodide. $TMPDASnCl_4$ exhibits a broad-band bluish-white-light emission (centered at 515 nm, full width at half-maximum (fwhm) = 193 nm) with the Commission Internationale de l′ Elairage (CIE) coordinates as (0.29, 0.34). Further, the correlated color temperature and color-rendering index were determined as 7617 K and 80.5, respectively. Based on the synthesis of new crystals, our work sheds light on the composition−structure−property relationship of hybrid Sn(II)-based halide perovskites.

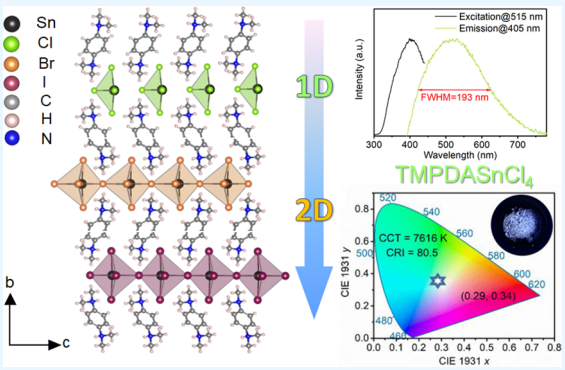

INTRODUCTION

Low-dimensional hybrid lead halide perovskites have exhibited multiple advantages including diverse structures, tunable optical gaps, and improved ambient stability compared to their three-dimensional (3D) analogues,[1−6] which make them extensively attractive for various optoelectronic applications such as solar cells,[7] lasers,[8] photodetection,[9] light-emitting diodes,[10] and dielectric switching.[11] Particularly, two-dimensional (2D) Pb-based perovskites have also emerged as excellent luminescent materials for solid-state lighting and displaying.[12−14] Owing to the structural quantum confinement and formation of self-trapped excitons (STEs), the 2D Pb-based perovskites can emit intense photoluminescence (PL) across the whole visible spectral region, which can even realize the single-component white-light emission to replace the commercial mixed phosphors containing rare earth metals.[15−20] Dohner et al. firstly reported the broad-band white-light emission in (100)-oriented 2D (N-MEDA)$PbBr_4$ (N-MPDA = *N*-methylpropane-1,3-diammonium) and (110)-oriented 2D (N-MEDA)$PbBr_4$ (N-MPDA = *N*-methylethane-1,2-diammonium).[21] Mao et al. also described the tunable white-light emission in a multilayered Pb halide system $(CH_3CH_2NH_3)_4Pb_3Br_{10-x}Cl_x$.[22] However, the toxicity of Pb still greatly impedes the commercial application of these 2D Pb-based halide perovskite materials.

Considering that Sn^{2+} is a nontoxic component with the same electronic configuration as Pb^{2+}, eco-friendly Sn(II)-based perovskites have been considered as ideal substitutions for Pb-based perovskites.[23−26] Focusing on the field of luminescence, Lanzetta et al. reported the first example of the Sn(II)-based perovskite LED with 2D $(PEA)_2SnI_4$ (PEA = phenylethylammonium) as the red emitter.[23] Subsequent works demonstrated that the luminescent properties of 2D Sn-based iodide can be readily tuned by anions or a spacer cation substitution strategy.[27,28] Further, strong yellow photoluminescence (PL) was discovered in the tin bromide perovskites $(OCTAm)_2SnBr_4$ (OCTAm = octylammonium)

Received: February 25, 2024
Revised: April 24, 2024
Accepted: April 25, 2024
Published: May 8, 2024

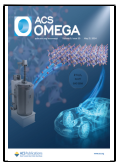

and $ODASnBr_4$ (ODA = 1,8-diaminooctane), both of which could exhibit near-unit photoluminescence quantum yields (PLQYs) and ultralong lifetimes.[24,29] A mixed-solvent strategy was also utilized to synthesize Sn(II) iodide perovskites $(BA)_2MA_{n-1}Sn_nI_{3n+1}$ with high phase purity, and the crystals exhibited excellent lasing performance.[30] Very recently, strong exciton localization effect was induced in $(OA)_2SnI_4$ by a large amount of Sn vacancies, resulting in the evidently increased PLQY (~64%) of orange light emission.[31] However, despite the advances in photoluminescence efficiency, the members of low-dimensional hybrid Sn(II)-based halide perovskites are still limited compared to their Pb counterparts, especially for the chlorides that are barely reported.[32,33] This issue leads to the deficient fundamental understanding of the halogen-structure−optical property relationship in hybrid Sn(II)-based perovskites, which hinders the rational design of these lead-free photoelectric materials.

In this work, N,N,N′,N′-tetramethyl-1,4-phenylenediamine (abbreviated as TMPDA) is used as the organic precursor to synthesize the hybrid Sn(II)-based halide perovskites. It is very impressive that a series of hybrid Sn(II) perovskites $TMPDASnX_4$ (X = Cl, Br, I) have been obtained by tuning the feeding ratio of raw materials. To our knowledge, this is the first time that the hybrid Sn(II)-based perovskites including chloride, bromide, and iodide are successfully synthesized with the identical organic ligand. Based on the structure analysis, highly distorted $[SnX_6]$ octahedra were observed in all three tin halides, and an unusual structural evolution was revealed from an actual one-dimensional (1D) five-coordinated configuration in chloride to 2D perovskite type in bromide and iodide. The halogen dependence of structure, stability, and optical properties of $TMPDASnX_4$ (X = Cl, Br, I) was investigated. Under UV light, $TMPDASnCl_4$ exhibits a broad-band bluish-white-light emission with a full width at half-maximum (fwhm) of 193 nm.

EXPERIMENTAL SECTION

Materials. N,N,N′,N′-Tetramethyl-1,4-phenylenediamine ($C_{10}H_{16}N_2$, 98%, Acros Organics), tin(II) chloride ($SnCl_2$, 99.99%, Macklin), tin(II) bromide ($SnBr_2$, 99%, Aladdin), tin(II) iodide (SnI_2, 99.999%, Bidepharm), hypophosphorous acid (H_3PO_2, 50% weight in water, Aladdin), hydrochloric acid (HCl, 36% weight in water, Aladdin), hydrobromic acid (HBr, 48% weight in water, Aladdin), and hydroiodic acid (HI, 47% weight in water, Macklin) were used for sample synthesis in this work. All of the chemicals were used as purchased without further purification.

Synthesis of $TMPDASnX_4$ (X = Cl, Br, and I). For $TMPDASnCl_4$ crystals, the synthetic route was performed with the molar ratio between TMPDA and $SnCl_2$ as 2:1. Typically, a mixture of 2 mmol of TMPDA (328.7 mg) and 1 mmol of $SnCl_2$ (189.6 mg) was placed in a bottle containing 2.5 mL of HCl and 1 mL of H_3PO_2. A light brown transparent solution was obtained with continuous magnetic stirring at 110 °C. The solution was then slowly cooled down to 30 °C with the rate of 1 °C/h. The chloride crystals were finally obtained by filtration. $TMPDASnBr_4$ and $TMPDASnI_4$ crystals were synthesized by a similar process, but a different molar ratio between TMPDA and SnX_2 as 1:1 is required, rather than 2:1.

Characterization. Single-crystal X-ray diffraction (SCXRD) measurements were performed on a Bruker APEX-II CCD diffractometer and determined at 150 K. The structure was analyzed using a direct method and refined using the Olex2 package, and the space group and twin law were checked using PLATON.[34,35] Powder X-ray diffraction (PXRD) was collected at room temperature on a PANalytical Empyrean diffractometer equipped with Cu Kα radiation (λ = 1.541 Å). The morphology of the samples was investigated via Regulus8100 scanning electron microscopy (SEM). Component analysis was performed by energy-dispersive X-ray spectroscopy (EDS). X-ray photoelectron spectroscopy (XPS) studies were performed by using a Thermo Scientific K-Alpha spectrometer. UV−vis reflectance spectroscopy was performed by using a Shimadzu UV-3600 UV−vis-NIR spectrometer. PL spectra and PL lifetimes were obtained using a PLSP920 fluorescence spectrophotometer equipped with a PMT detector at room temperature and a 150 W Xe900 lamp as the excitation source.

Calculation. All calculations were performed using density functional theory (DFT) using the Vienna Ab initio Simulation Package (VASP) and the projector-augmented wave (PAW) scheme. Perdew−Burke−Ernzerhof generalized gradient approximation (PBE-GGA) was used for the exchange correlation functional.[36−38] The wave functions were expanded into plane waves up to a cutoff energy of 600 eV. The structures were relaxed with an energy convergence criterion of 10^{-5} eV, ensuring that the maximum force on an atom was <0.02 eV $Å^{-1}$.

RESULTS AND DISCUSSION

Synthesis and Crystal Structure. Single crystals of all three Sn-based perovskites were synthesized by directly reacting the raw materials TMPDA and SnX_2 (X = Cl, Br, I) in a mixture solution of HX and H_3PO_2, as shown in Figure 1a.

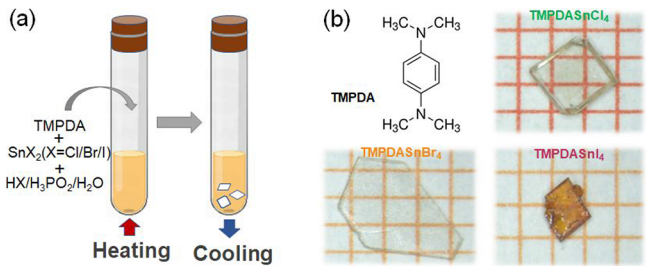

Figure 1. (a) Schematic illustration of the synthesis of $TMPDASnX_4$ (X = Cl, Br, and I). (b) Structural formula of TMPDA and optical images of $TMPDASnX_4$.

It should be mentioned that the chloride crystal was first prepared with the molar ratio between TMPDA and $SnCl_2$ as 2:1, but the synthesis of bromide and iodide failed using the same molar ratio. When the molar content of TMPDA was reduced to the same level as $SnBr_2$ (SnI_2), the crystals were successfully obtained, suggesting that the feeding ratio of raw materials is dependent on the halogen to synthesize the Sn(II)-based hybrid perovskites. As shown in Figure 1b, all of the products are plate-like and transparent. The chloride and bromide are colourless and the iodide is light brown. The SEM images of all three crystals are shown in Figure S1, together with the EDS spectrum, showing the ratio of Sn and X as around 1:4.

The crystal structures of these three Sn(II)-based perovskites were determined by SCXRD, and the obtained crystallographic data are presented in Tables S1−S7. According to the low R values, the three solved structures

https://doi.org/10.1021/acsomega.4c01835
ACS Omega 2024, 9, 22352−22359

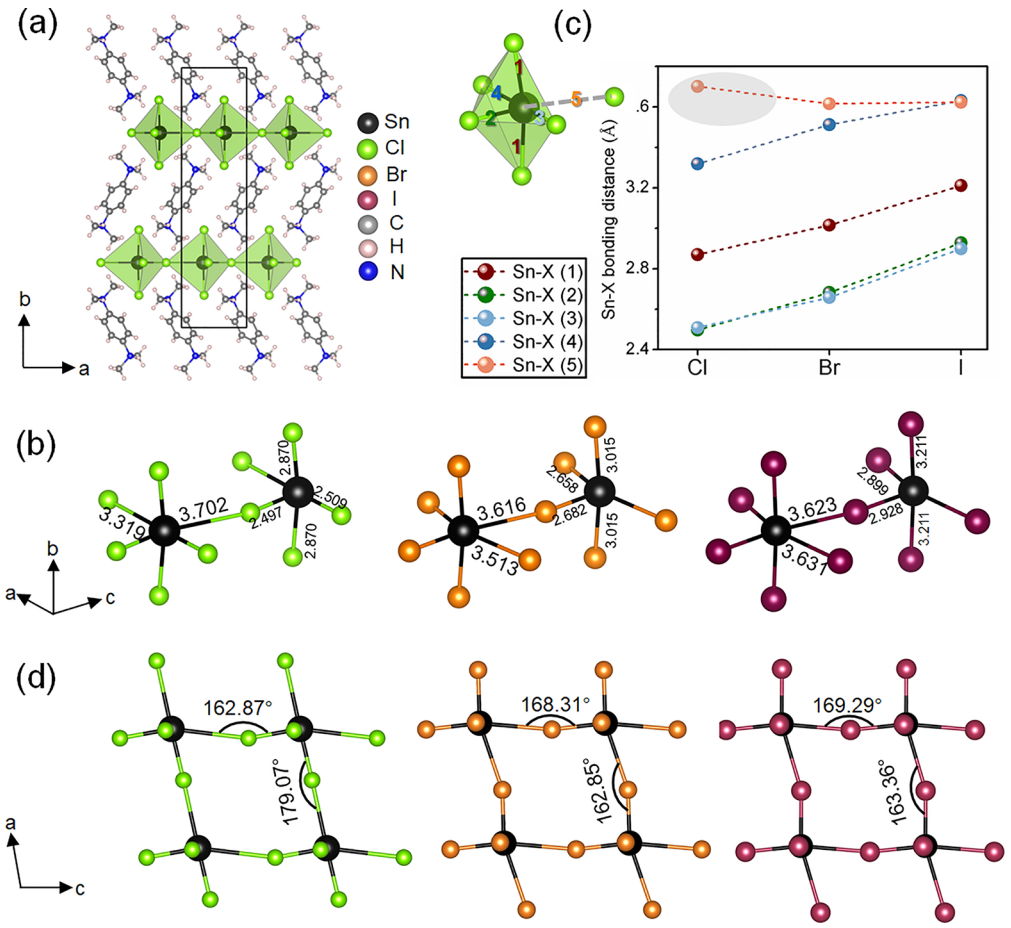

Figure 2. (a) Crystal structure of $TMPDASnCl_4$. The unit cell is shown by a black rectangle. (b) Sn−X bonding lengths in $TMPDASnX_4$ (X = Cl, Br, I). (c) Variation trend of the Sn−X bonding distances in order from $TMPDASnCl_4$ to $TMPDASnBr_4$ to $TMPDASnI_4$. Inset shows the actual five-coordinated pyramid configuration of the pseudooctahedron in $TMPDASnCl_4$ with the longest Sn−Cl bond unformed. (d) In-plane Sn−X−Sn bond angles in $TMPDASnX_4$ (X = Cl, Br, I).

Table 1. Summary of Structural Distortion Parameters, Band Gaps, and PL Characteristics for $TMPDASnCl_4$, $TMPDASnBr_4$, and $TMPDASnI_4$ and Other Reported Sn-Based 2D Halides[26,41]

compound	Δd	σ^2	E_g (eV)	λ_{em} (nm)	PLQY (%)	ref.
$(PEA)_2SnI_4$	3.44×10^{-5}	1.31	2.02	624	1.06	26
$(BA)_2SnI_4$	4.48×10^{-5}	4.96	2.04	621	0.22	26
$(HA)_2SnI_4$	\	\	2.05	617	0.54	26
$(OA)_2SnI_4$	\	\	2.06	615	0.17	26
$(C_6H_{13}NH_3)_2SnBr_4$	\	\	3.48	618	35.0	41
$(C_{12}H_{25}NH_3)_2SnBr_4$	\	\	3.20	603	60.2	41
$(C_{18}H_{35}NH_3)_2SnBr_4$	\	\	3.36	623	51.5	41
$TMPDASnCl_4$	2.12×10^{-2}	83.25	3.5	515	<1	this work
$TMPDASnBr_4$	1.44×10^{-2}	76.45	3.19	435	\	this work
$TMPDASnI_4$	8.11×10^{-3}	63.69	2.35	408	\	this work

are considered reliable, which are all isostructural in a monoclinic system, $P2_1/m$ (No. 11) space group. The chemical compositions are refined as $(C_{10}H_{16}N_2)SnX_4$ (X = Cl, Br, I) based on SCXRD, which are in agreement with the EDS results. As a representative, the structures of $TMPDASnCl_4$ are shown in Figure 2a, showing a typical (100)-oriented 2D perovskite nature with corner-sharing $[SnCl_6]$ octahedral configuration. The $[TMPDA]^{2+}$ cations stack alternately with the inorganic layers, and the benzene rings are highly ordered, with the aromatic planes parallel to each other in organic ligands. The detailed Sn−X bonding distances are shown in Figure 2b, and it can be seen that the two axial Sn-X bonds are equal with the bonding length as 2.870, 3.015, and 3.211 Å for chloride, bromide, and iodide, respectively. It is worth noting that the four equatorial Sn−X bonds in each 2D Sn-based perovskite exhibit strong distortion with two extremely long Sn−X distances, especially in $TMPDASnCl_4$, implying that the chemical bond may not be formed between the Cl and Sn atoms. To further investigate the bonding condition in this Sn(II)-based perovskite system, the five Sn−X bonding lengths in three hybrid halides are plotted in Figure 2c, where the axial Sn−X bonds (Sn−X (1)) and two short equatorial bonds

https://doi.org/10.1021/acsomega.4c01835
ACS Omega 2024, 9, 22352−22359

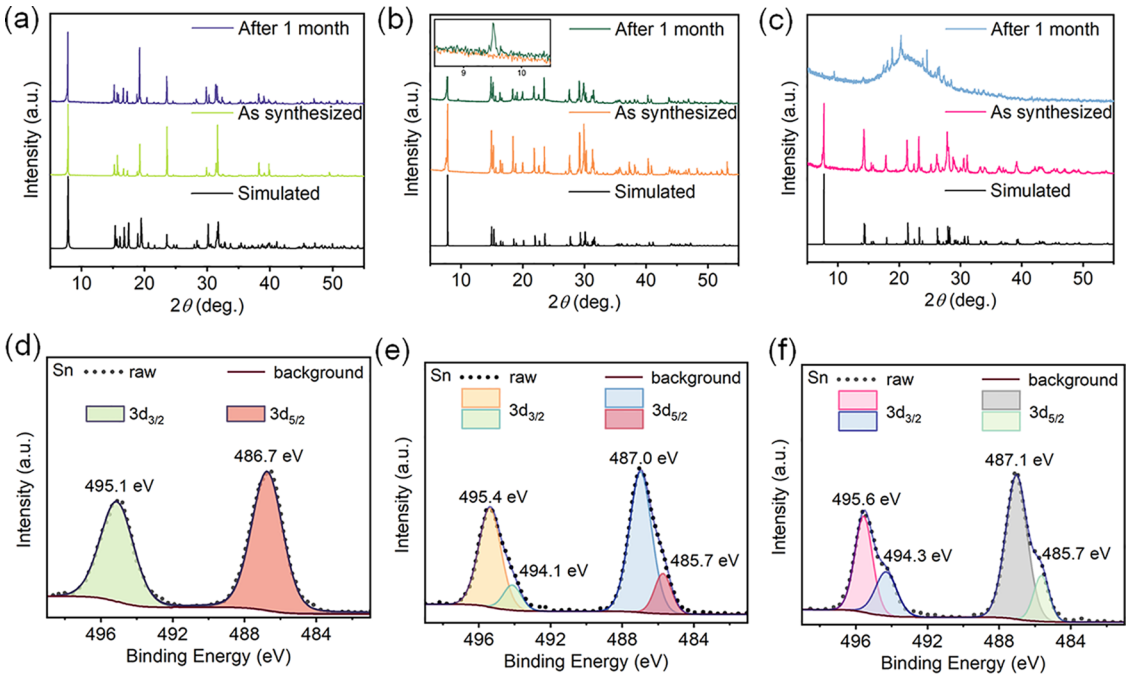

Figure 3. PXRD patterns of (a) $TMPDASnCl_4$, (b) $TMPDASnBr_4$, and (c) $TMPDASnI_4$ compared to the simulated ones from SCXRD. High-resolution XPS spectra of Sn for (d) $TMPDASnCl_4$, (e) $TMPDASnBr_4$, and (f) $TMPDASnI_4$.

(Sn−X (2) and Sn−X (3)) are monotonously elongated from chloride to bromide and then to iodide due to the increased radius of anions. Focusing on the two long Sn−X bonds, the Sn−X (4) bond is still monotonous as expected, but the Sn−X (5) bond shows an abnormal trend (marked by gray color) with the bonding distance decreased from $TMPDASnCl_4$ to $TMPDASnBr_4$, indicating that this bond does not actually form in the chloride. Hence, the inorganic polyhedron in $TMPDASnCl_4$ is a five-coordinated $[SnCl_5]$ pyramid, as shown in the inset of Figure 2c, leading to a one-dimensional (1D) structure in this compound. For $TMPDASnBr_4$ and $TMPDASnI_4$, the structures are still 2D, which are isostructural with their Pb analogue $TMPDAPbBr_4$ as reported previously.[39] Furthermore, the structural distortion of $[SnX_6]^{4-}$ octahedra is also evaluated by calculating the bond length distortion Δd and octahedral angle variance σ^2 using the following equations[40]:

$$\Delta d = \frac{1}{6}\sum_{i}^{6}\left(\frac{d_i - d}{d}\right)^2 \quad (1)$$

$$\sigma^2 = \frac{1}{11}\sum_{i}^{12}(\theta_i - 90^\circ)^2 \quad (2)$$

where d is the average Sn−X bond length, d_i is the individual Sn−X bond length, and θ_i is the individual bond angle. The Δd and σ^2 of $[SnX_6]^{4-}$ octahedral in three halides are listed in Table 1, and it is found that all the three compounds are highly distorted, suggesting the strong structural strain in them. It is noted that the high distortion was also observed in $TMPDAPbBr_4$ as previously reported,[39] but the distortion degree is relatively smaller than that of its Sn analogue. The in-plane Sn−X−Sn bond angles in three compounds were also plotted in Figure 2d, where the angles decreased along the a direction (179.07, 162.85, and 163.36°) but increased along c (162.87, 168.31, and 169.29°) from chloride to bromide and then to iodide. The structural distortion parameters of some reported 2D Sn-based halides are also given in Table 1 for comparison.

Stability and Chemical States. PXRD patterns of the three halide samples were measured based on the grounded powders, and the results are shown in Figure 3a−c. The experimental PXRD patterns agreed fairly well with the simulated patterns from SCXRD results, indicating the high purity of the samples. The stability of these tin halides in ambient conditions was also studied by measuring the PXRD patterns of the samples that were exposed to air for 1 month. No visible change could be observed in the pattern of $TMPDASnCl_4$ compared to its fresh sample, indicating the satisfactory stability of this chloride. However, a diffraction peak from unknown impurity appears for $TMPDASnBr_4$ after one month exposure (see the peak at around 9.5° as shown in the inset), and this scenario is intensified in $TMPDASnI_4$, which totally decomposed after exposure to air. This demonstrates that the ambient stability is declined from chloride to bromide and iodide, despite the same rigid organic cations in their structures.

XPS measurement was carried out to study the chemical states of Sn in the three samples. The full XPS spectra are shown in Figure S2, confirming the coexistence of Sn, Cl(Br/I), C, and N elements in the crystals. Figure 3d shows the high-resolution XPS spectra of Sn for $TMPDASnCl_4$, and refined peaks located at 486.7 and 495.1 eV are ascribed to Sn^{2+} $3d_{3/2}$ and $3d_{5/2}$,[26] indicating the pure bivalence of Sn in chloride. However, these peaks shifted to the higher binding energy ranges in bromide (487.0 and 495.4 eV) and iodide (487.1 and 495.6 eV) shown in Figure 3e,f, suggesting the higher chemical valence of Sn in these two tin halides. In addition, the peak of Sn^{0+} located at 485.7 eV was also observed for $TMPDASnBr_4$ and $TMPDASnI_4$,[42] further confirming the decomposition of these two compounds. In brief, the XPS results confirm the declined ambient stability of the $TMPDASnBr_4$ and

https://doi.org/10.1021/acsomega.4c01835
ACS Omega 2024, 9, 22352−22359

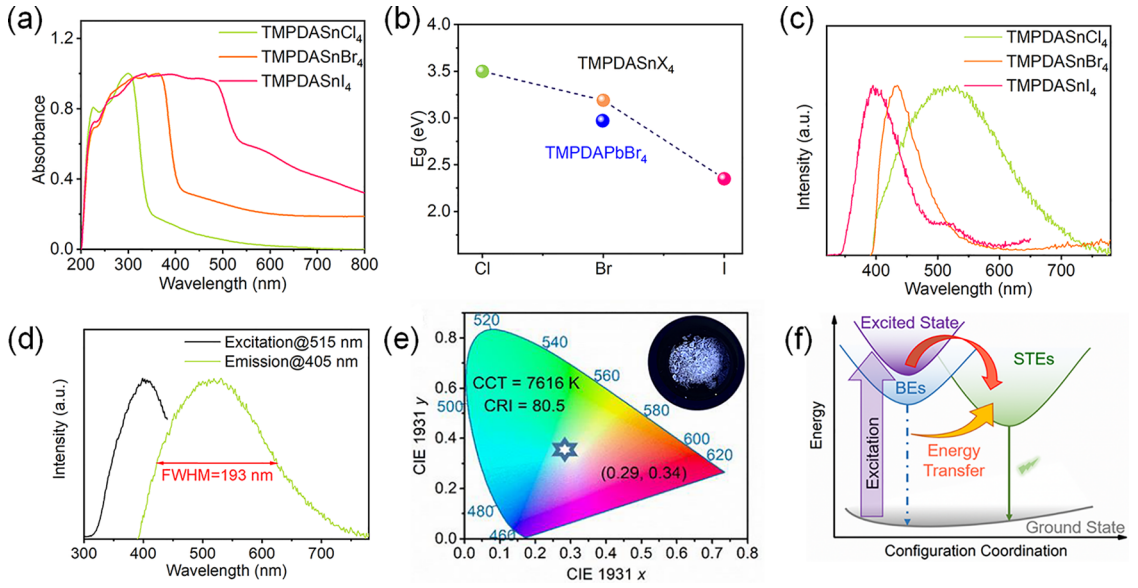

Figure 4. (a) UV−vis absorption spectra, (b) extracted band gap values, and (c) emission spectra of $TMPDASnX_4$ (X = Cl, Br, I). (d) Excitation and emission spectra and (e) CIE coordinates of $TMPDASnCl_4$. Inset is the photograph of crystals under 365 nm UV light, showing bluish white light. (f) Schematic illustration of the emission mechanism for $TMPDASnCl_4$.

$TMPDASnI_4$ crystals, which are consistent with the PXRD results.

Optical Properties. UV−vis absorption spectra of the three compounds are shown in Figure 4a. As expected, the adsorption band edge of $TMPDASnX_4$ shows the red shift in order from Cl to Br and then to I. Meanwhile, the absorption band tail can also be observed for three samples especially for the iodide, which is mainly associated with intense distortion of the lattice.[43,44] The band gaps of $TMPDASnX_4$ were extracted by Tauc plots, as shown in Figure S3,[45] where the chloride was treated as an indirect gap semiconductor, while the bromide and iodide were treated as the direct one which is based on the theoretical calculation, and the details can be seen in the next section. The results are plotted in Figure 4b, together with the band gap of $TMPDAPbBr_4$ taken from the literature.[39] It can be seen that the optical band gap of $TMPDASnCl_4$ is determined as 3.50 eV, and it reduces for ∼0.3 eV in $TMPDASnBr_4$ (3.19 eV), supporting the transparent nature shown in Figure 1b. It is also noted that compared to its Pb-based analogue (2.93 eV),[39] the Sn-based bromide exhibits a larger optical band gap due to the lower orbital energy of Sn(5s) compared to that of Pb(6s). For $TMPDASnI_4$, the band gap is significantly reduced to 2.35 eV, corresponding to the light brown color of the crystals. The calculated band structures of $TMPDASnX_4$ will be discussed in detail below.

The PL spectra of $TMPDASnX_4$ are plotted in Figure 4c with peaks centered at 515, 435, and 408 nm for chloride, bromide, and iodide, respectively. The PL emissions of these three tin halides are all very weak. Interestingly, under 405 nm excitation (the best excitation wavelength as shown in Figure S4), the $TMPDASnCl_4$ crystals show a broad-band emission with the peak basically crossing the whole visible-light region (400−800 nm) with the fwhm as 193 nm (Figure 4d). The Commission Internationale de lÉclairage (CIE) coordinates of $TMPDASnCl_4$ were determined to be (0.29, 0.34), which is located on the white-light region, as shown in Figure 4e, and the crystal as shown in the inset exhibits a bluish-white-light emission. Additionally, $TMPDASnCl_4$ corresponds to a correlated color temperature (CCT) of 7616 K and a color rendering index (CRI) of 80.5. However, the internal PLQY of $TMPDASnCl_4$ is very low (<1%) upon 405 nm excitation (Figure S5), which may be resulted from the defect state and strong exciton−phonon coupling.[28] The luminescence lifetime of $TMPDASnCl_4$ was determined by using time-resolved PL decays (Figure S6), and the data can be fitted by a single exponential equation, resulting in a lifetime of 2.55 ns. Based on our structural analysis, we speculate that the broad-band emission of $TMPDASnCl_4$ could be ascribed to its highly distorted octahedral geometry associated with self-trapped excitons (STEs). It should be mentioned that the weak emission of the bromide $TMPDASnBr_4$ is contradictory with the previous works, in which the 2D hybrid Sn-based bromides generally show strong yellow emission.[24,46] This is probably due to the incompetent stability of $TMPDASnBr_4$, but the specific reason is still unclear at the current stage.

To investigate the interaction between the inorganic and organic moieties in $TMPDASnCl_4$, the PL spectrum of TMPDA was also measured. Upon 358 nm excitation, the organic TMPDA shows an emission band at around 382 nm, as shown in Figure S7, which overlaps with the absorption band tail of $TMPDASnCl_4$. This spectral overlap implies the energy transfer behavior in $TMPDASnCl_4$, in which the organic cations act as donors and the inorganic polyhedra act as an acceptor. A similar scenario was also observed in the Pb isologue $TMPDAPbBr_4$.[39] The UV−vis absorption spectra of the organic precursor in Figure S8 show an absorption peak in the high-energy region (∼300 nm), which corresponds to the high energy emission in Figure S7. The PL lifetime of the organic precursor was also measured (Figure S9), and the value (4.96 ns) is different from that of $TMPDASnCl_4$.

Based on these results, the emission mechanism of $TMPDASnCl_4$ can be described in Figure 4f. The electrons in the ground state were immediately promoted to the excited states of both organic and inorganic moieties upon photo-generation, inducing an electron transition crossing the

https://doi.org/10.1021/acsomega.4c01835
ACS Omega 2024, 9, 22352−22359

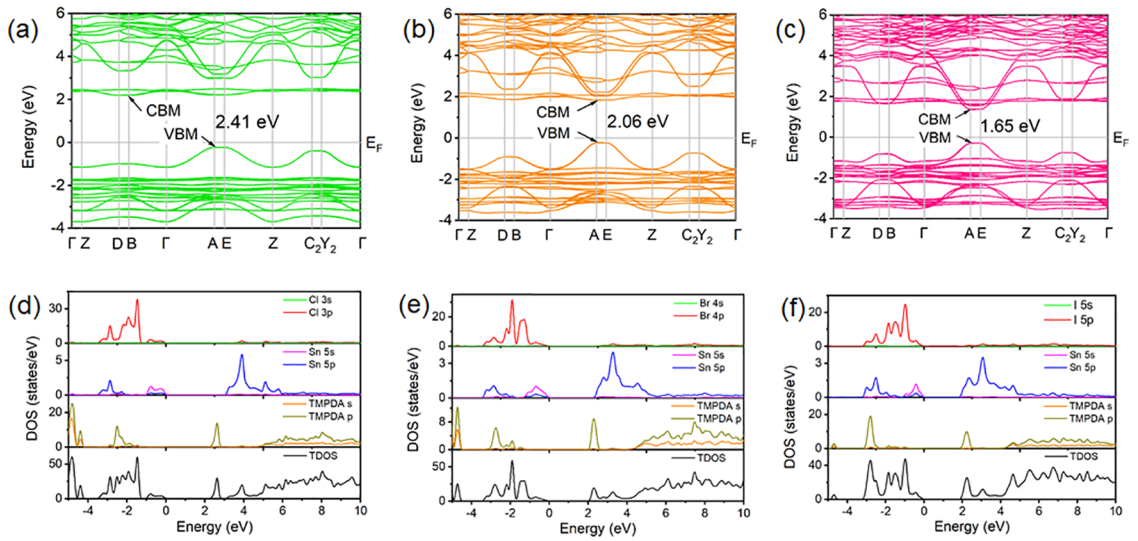

Figure 5. Electronic band structures for (a) $TMPDASnCl_4$, (b) $TMPDASnBr_4$, and (c) $TMPDASnI_4$. Total and partial DOS of (d) $TMPDASnCl_4$, (e) $TMPDASnBr_4$, and (f) $TMPDASnI_4$.

electronic band. The high-energy emission caused by bound excitons (BEs) in $[TMPDA]^{2+}$ was quenched due to the energy transfer. In the meantime, the $[SnCl_6]^{2-}$ octahedra undergo distortion, and the STEs were formed within a short period of time when the confined excitons promptly reorganized and were self-trapped by the distorted lattice. Finally, the radiative transition of these STEs led to the broad-band bluish-white-light emission in $TMPADSnCl_4$.

Theoretical Calculations. The electronic structures and density of states (DOS) of $TMPDASnX_4$ were calculated. As shown in Figure 5a−c, $TMPDASnCl_4$ shows a indirect band gap with a theoretical value of 2.41 eV, while $TMPDASnBr_4$ and $TMPDASnI_4$ show an direct bandgap characteristic with the calculated band gaps of 2.06 and 1.65 eV, respectively. As shown in Figure 5d−f, the valence band maximum (VBM) of the three Sn halides is mainly contributed by the halogen p and Sn 5s orbitals from the inorganic moiety. For the conduction band minimum (CBM), the electronic states from the organic TMPDA locate at the same energy level range with those from the inorganic halogen p 3p and Sn 5p states, suggesting the hybridization between the organic ligand and $[SnX_6]$ octahedra.[39,47] These hybrid states indicate the strong resonance interaction between the organic and inorganic moieties, leading to the aforementioned energy transfer. Based on our calculation, the Forster resonant energy transfer (FRET) may occur between the organic and inorganic ligands, and the broad-band emission in $TMPDASnCl_4$ could be related to this FRET.

CONCLUSIONS

In this work, we used the same organic cation to synthesize the hybrid Sn(II)-based chloride, bromide, and iodide perovskite materials. Three Sn(II) halide perovskites $TMPDASnX_4$ (X = Cl, Br, I) were synthesized, and the evolution of their structure and optical properties was studied depending on the change of halogen. The structural analysis indicated that all three halides adopt the monoclinic lattice, $P2_1/m$ space group, showing the typical (100)-oriented 2D perovskite structure with highly distorted $[SnX_6]$ octahedra. Unexpectedly, the detailed analysis on the Sn−X bonding length demonstrated that the inorganic ligand in $TMPDASnCl_4$ has a five-coordinate configuration due to the unbonded nature of one Sn−Cl pair. $TMPDASnCl_4$ exhibited a broad-band bluish-white-light emission (centered at 515 nm, fwhm = 193 nm) with CIE coordinates of (0.29, 0.34), and the correlated color temperature and color rendering index were determined as 7617 K and 80.5, respectively. Our work provides an interesting series of new compounds to deeply understand the halogen-structure−property relationship of hybrid Sn(II)-based halide perovskites.

ASSOCIATED CONTENT

Supporting Information

The Supporting Information is available free of charge at https://pubs.acs.org/doi/10.1021/acsomega.4c01835.

Crystallographic data; atomic coordinates; displacement parameters; anisotropic displacement parameters; bond distances and bond angles; EDS results; XPS spectra; extracted band gaps; emission spectra at different excitation wavelengths; PLQY experimental data; time-resolved decay curves of $TMPDASnCl_4$; and PL spectra of the organic precursor (PDF)

Crystal data and structure refinement of $TMPDASnCl_4$ (CIF)

Crystal data and structure refinement of $TMPDASnBr_4$ (CIF)

Crystal data and structure refinement of $TMPDASnI_4$ (CIF)

Accession Codes

CCDC 2156620, 2256629, and 2256630 contain the supplementary crystallographic data for this paper. These data can be obtained free of charge via www.ccdc.cam.ac.uk/data_request/ cif, or by emailing data_request@ccdc.cam.ac.uk, or by contacting The Cambridge Crystallographic Data Centre, 12 Union Road, Cambridge CB2 1EZ, UK; fax: + 44 1223 336033.

AUTHOR INFORMATION

Corresponding Authors

Jiawei Lin − *Department of Chemistry, School of Chemistry and Biological Engineering, University of Science and Technology Beijing, Beijing 100083, China;* Present

https://doi.org/10.1021/acsomega.4c01835
ACS Omega 2024, 9, 22352−22359

Address: Department of Chemistry, Southern University of Science and Technology, Shenzhen, Guangdong 518055, China (J.L.); Email: linjw@sustech.edu.cn

Zhongnan Guo − *Department of Chemistry, School of Chemistry and Biological Engineering, University of Science and Technology Beijing, Beijing 100083, China;* orcid.org/0000-0003-4907-4679; Email: guozhongn@ustb.edu.cn

Authors

Ruonan Yao − *Department of Chemistry, School of Chemistry and Biological Engineering, University of Science and Technology Beijing, Beijing 100083, China*

Kunjie Liu − *The Beijing Municipal Key Laboratory of New Energy Materials and Technologies, School of Materials Sciences and Engineering, University of Science and Technology Beijing, Beijing 100083, China*

Yuanchang Xu − *Department of Chemistry, School of Chemistry and Biological Engineering, University of Science and Technology Beijing, Beijing 100083, China*

Boyi Xiao − *Department of Chemistry, School of Chemistry and Biological Engineering, University of Science and Technology Beijing, Beijing 100083, China*

Jing Zhao − *The Beijing Municipal Key Laboratory of New Energy Materials and Technologies, School of Materials Sciences and Engineering, University of Science and Technology Beijing, Beijing 100083, China;* orcid.org/0000-0002-8000-5973

Quanlin Liu − *The Beijing Municipal Key Laboratory of New Energy Materials and Technologies, School of Materials Sciences and Engineering, University of Science and Technology Beijing, Beijing 100083, China;* orcid.org/0000-0003-3533-7140

Wenxia Yuan − *Department of Chemistry, School of Chemistry and Biological Engineering, University of Science and Technology Beijing, Beijing 100083, China;* orcid.org/0000-0002-3521-3538

Complete contact information is available at: https://pubs.acs.org/10.1021/acsomega.4c01835

Notes

The authors declare no competing financial interest.

■ ACKNOWLEDGMENTS

The financial supports by the National Natural Science Foundation of China (No. 52271199), the National Key R&D Program of China (No. 2020YFA0406202), and the Fundamental Research Funds for the Central Universities (FRF-EYIT-23-04) are gratefully acknowledged.

■ REFERENCES

(1) Mao, L.; Stoumpos, C. C.; Kanatzidis, M. G. Two-Dimensional Hybrid Halide Perovskites: Principles and Promises. *J. Am. Chem. Soc.* **2019**, *141* (3), 1171−1190.

(2) Grancini, G.; Nazeeruddin, M. K. Dimensional tailoring of hybrid perovskites for photovoltaics. *Nat. Rev. Mater.* **2019**, *4* (1), 4−22.

(3) Lei, Y.; Chen, Y.; Zhang, R.; Li, Y.; Yan, Q.; Lee, S.; Yu, Y.; Tsai, H.; Choi, W.; Wang, K.; Luo, Y.; Gu, Y.; Zheng, X.; Wang, C.; Wang, C.; Hu, H.; Li, Y.; Qi, B.; Lin, M.; Zhang, Z.; Dayeh, S. A.; Pharr, M.; Fenning, D. P.; Lo, Y.-H.; Luo, J.; Yang, K.; Yoo, J.; Nie, W.; Xu, S. A fabrication process for flexible single-crystal perovskite devices. *Nature* **2020**, *583* (7818), 790−795.

(4) Song, Z.; Zhao, J.; Liu, Q. Luminescent perovskites: recent advances in theory and experiments. *Inorg. Chem. Front.* **2019**, *6* (11), 2969−3011.

(5) Babu, R.; Giribabu, L.; Singh, S. P. Recent Advances in Halide-Based Perovskite Crystals and Their Optoelectronic Applications. *Cryst. Growth Des.* **2018**, *18* (4), 2645−2664.

(6) Mao, L.; Teicher, S. M. L.; Stoumpos, C. C.; Kennard, R. M.; DeCrescent, R. A.; Wu, G.; Schuller, J. A.; Chabinyc, M. L.; Cheetham, A. K.; Seshadri, R. Chemical and Structural Diversity of Hybird Layered Double Perovskite Halides. *J. Am. Chem. Soc.* **2019**, *141* (48), 19099−19109.

(7) Tsai, H.; Nie, W.; Blancon, J.-C.; Stoumpos, C. C.; Asadpour, R.; Harutyunyan, B.; Neukirch, A. J.; Verduzco, R.; Crochet, J. J.; Tretiak, S.; Pedesseau, L.; Even, J.; Alam, M. A.; Gupta, G.; Lou, J.; Ajayan, P. M.; Bedzyk, M. J.; Kanatzidis, M. G.; Mohite, A. D. High-efficiency two-dimensional Ruddlesden−Popper perovskite solar cells. *Nature* **2016**, *536* (7616), 312−316.

(8) Tan, Z.; Wu, Y.; Hong, H.; Yin, J.; Zhang, J.; Lin, L.; Wang, M.; Sun, X.; Sun, L.; Huang, Y.; Liu, K.; Liu, Z.; Peng, H. Two-Dimensional $(C_4H_9NH_3)_2PbBr_4$ Perovskite Crystals for High-Performance Photodetector. *J. Am. Chem. Soc.* **2016**, *138* (51), 16612−16615.

(9) Qin, C.; Sandanayaka, A. S. D.; Zhao, C.; Matsushima, T.; Zhang, D.; Fujihara, T.; Adachi, C. Stable room-temperature continuous-wave lasing in quasi-2D perovskite films. *Nature* **2020**, *585* (7823), 53−57.

(10) Yang, S.; Niu, W.; Wang, A. L.; Fan, Z.; Chen, B.; Tan, C.; Lu, Q.; Zhang, H. Ultrathin Two-Dimensional Organic−Inorganic Hybrid Perovskite Nanosheets with Bright, Tunable Photoluminescence and High Stability. *Angew. Chem., Int. Ed.* **2017**, *56* (15), 4252−4255.

(11) Jia, Q.-Q.; Tong, L.; Lun, M.-M.; Fu, D.-W.; Zhang, T.; Lu, H.-F. Two-Dimensional Organic−Inorganic Hybrid Materials with Dielectric Switching and Photoluminescence Properties. *Cryst. Growth Des.* **2022**, *22* (5), 2799−2805.

(12) Byun, J.; Cho, H.; Wolf, C.; Jang, M.; Sadhanala, A.; Friend, R. H.; Yang, H.; Lee, T. W. Efficient Visible Quasi-2D Perovskite Light-Emitting Diodes. *Adv. Mater.* **2016**, *28* (34), 7515−7520.

(13) Xing, J.; Zhao, Y.; Askerka, M.; Quan, L. N.; Gong, X.; Zhao, W.; Zhao, J.; Tan, H.; Long, G.; Gao, L.; Yang, Z.; Voznyy, O.; Tang, J.; Lu, Z.-H.; Xiong, Q.; Sargent, E. H. Color-stable highly luminescent sky-blue perovskite light-emitting diodes. *Nat. Commun.* **2018**, *9* (1), 3541.

(14) Tao, K.; Han, S.; Ji, C.; Liu, X.; Wu, Z.; Zhang, J.; Luo, J.; Sun, Z. Structural Phase Transition and Switchable Dielectric Properties of a Unique Two-Dimensional Organic−Inorganic Hybrid Perovskite Compound $[C_6H_{11}NH_2CH_3]_4Pb_3I_{10}$. *Cryst. Growth Des.* **2018**, *18* (12), 7316−7322.

(15) Dohner, E. R.; Jaffe, A.; Bradshaw, L. R.; Karunadasa, H. I. Intrinsic White-Light Emission from Layered Hybrid Perovskites. *J. Am. Chem. Soc.* **2014**, *136* (38), 13154−13157.

(16) Hu, T.; Smith, M. D.; Dohner, E. R.; Sher, M.-J.; Wu, X.; Trinh, M. T.; Fisher, A.; Corbett, J.; Zhu, X. Y.; Karunadasa, H. I.; Lindenberg, A. M. Mechanism for Broadband White-Light Emission from Two-Dimensional (110) Hybrid Perovskites. *J. Phys. Chem. Lett.* **2016**, *7* (12), 2258−2263.

(17) Liu, Y.; Guo, J.; Zhou, H.; Li, C.; Guo, X. Correlating $\pi-\pi$ Stacking of Aromatic Diammoniums with Stability and Dimensional Reduction of Dion−Jacobson 2D Perovskites. *J. Am. Chem. Soc.* **2024**, *146* (12), 8198−8205.

(18) Chiara, R.; Morana, M.; Folpini, G.; Olivati, A.; Albini, B.; Galinetto, P.; Chelazzi, L.; Ciattini, S.; Fantechi, E.; Serapian, S. A.; Petrozza, A.; Malavasi, L. The templating effect of diammonium cations on the structural and optical properties of lead bromide perovskites: a guide to design broad light emitters. *J. Mater. Chem. C* **2022**, *10* (34), 12367−12376.

(19) Morana, M.; Kaiser, W.; Chiara, R.; Albini, B.; Meggiolaro, D.; Mosconi, E.; Galinetto, P.; Angelis, F. D.; Malavasi, L. Origin of Broad Emission Induced by Rigid Aromatic Ditopic Cations in Low-

Dimensional Metal Halide Perovskites. *J. Phys. Chem. Lett.* **2023**, *14* (35), 7860−7868.
(20) Cortecchia, D.; Neutzner, S.; Kandada, A. R. S.; Mosconi, E.; Meggiolaro, D.; Angelis, F. D.; Soci, C.; Petrozza, A. Broadband Emission in Two-Dimensional Hybrid Perovskites: The Role of Structural Deformation. *J. Am. Chem. Soc.* **2017**, *139* (1), 39−42.
(21) Dohner, E. R.; Hoke, E. T.; Karunadasa, H. I. Self-Assembly of Broadband White-Light Emitters. *J. Am. Chem. Soc.* **2014**, *136* (5), 1718−1721.
(22) Mao, L.; Wu, Y.; Stoumpos, C. C.; Traore, B.; Katan, C.; Even, J.; Wasielewski, M. R.; Kanatzidis, M. G. Tunable White-Light Emission in Single-Cation-Templated Three-Layered 2D Perovskites $(CH_3CH_2NH_3)_4Pb3Br_{10-x}Cl_x$. *J. Am. Chem. Soc.* **2017**, *139* (34), 11956−11963.
(23) Lanzetta, L.; Marin-Beloqui, J. M.; Sanchez-Molina, I.; Ding, D.; Haque, S. A. Two-Dimensional Organic Tin Halide Perovskites with Tunable Visible Emission and Their Use in Light-Emitting Devices. *ACS Energy Lett.* **2017**, *2* (7), 1662−1668.
(24) Wang, A.; Guo, Y.; Zhou, Z.; Niu, X.; Wang, Y.; Muhammad, F.; Li, H.; Zhang, T.; Wang, J.; Nie, S.; Deng, Z. Aqueous acid-based synthesis of lead-free tin halide perovskites with near-unity photoluminescence quantum efficiency. *Chem. Sci.* **2019**, *10* (17), 4573−4579.
(25) Jung, M.-H. The red light emission in 2D $(C_4SH_3CH_2NH_3)_2SnI_4$ and $(C_4OH_7CH_2NH_3)_2SnI_4$ perovskites. *Dalton. Trans.* **2021**, *50* (29), 10261−10274.
(26) Zhang, T.; Zhou, C.; Feng, X.; Dong, N.; Chen, H.; Chen, X.; Zhang, L.; Lin, J.; Wang, J. Regulation of the luminescence mechanism of two-dimensional tin halide perovskites. *Nat. Commun.* **2022**, *13* (1), 60.
(27) Chen, M.; Lin, J.; Hsu, C.; Chang, C.; Chiu, C.; Chen, H. M.; Chou, P. Strongly Coupled Tin-Halide Perovskites to Modulate Light Emission: Tunable 550−640 nm Light Emission (FWHM 36−80 nm) with a Quantum Yield of up to 6.4%. *Adv. Mater.* **2018**, *30* (20), No. 1706592.
(28) Wang, Z.; Wang, F.; Zhao, B.; Qu, S.; Hayat, T.; Alsaedi, A.; Sui, L.; Yuan, K.; Zhang, J.; Wei, Z.; Tan, Z. A. Efficient Two-Dimensional Tin Halide Perovskite Light-Emitting Diodes via a Spacer Cation Substitution Strategy. *J. Phys. Chem. Lett.* **2020**, *11* (3), 1120−1127.
(29) Zhang, L.; Yang, B.; Mei, S.; Zhu, Y.; Hu, R.; Zou, J. Highly luminescent broadband phosphors based on acid solvent coordinated two-dimensional layered tin-based perovskites. *J. Mater. Chem. C* **2022**, *10* (10), 3856−3862.
(30) Li, Y.; Zhou, H.; Xia, M.; Shen, H.; Wang, T.; Gao, H.; Sheng, X.; Han, Y.; Chen, Z.; Dou, L.; Zhu, H.; Shi, E. Phase-pure 2D tin halide perovskite thin flakes for stable lasing. *Sci. Adv.* **2023**, *9*, No. eadh0517.
(31) Chen, Y.; Wang, Z.; Wei, Y.; Liu, Y.; Hong, M. Exciton Localization for Highly Luminescent Two-Dimensional Tin-Based Hybrid Perovskites through Tin Vacancy Tuning. *Angew. Chem., Int. Ed.* **2023**, *62*, No. e202301684.
(32) Song, G.; Li, Z.; Gong, P.; Xie, R.; Lin, Z. Tunable White Light Emission in a Zero-Dimensional Organic−Inorganic Metal Halide Hybrid with Ultra-High Color Rendering Index. *Adv. Opt. Mater.* **2021**, *9* (11), No. 2002246.
(33) Sayer, I.; Dege, N.; Ghalla, H.; Naïli, H. Low pH-induced lone-pair activity in the hybrid $(C_6H_{10}N_2)[SnCl_3]Cl$: Chemical study and physical characterizations. *J. Mol. Struct.* **2022**, *1248*, No. 131403.
(34) Dolomanov, O. V.; Bourhis, L. J.; Gildea, R. J.; Howard, J. A. K.; Puschmann, H. OLEX2: a complete structure solution, refinement and analysis program. *J. Appl. Crystallogr.* **2009**, *42* (2), 339−341.
(35) Spek, A. J. Single-crystal structure validation with the program PLATON. *J. Appl. Crystallogr.* **2003**, *36*, 7−13.
(36) Hohenberg, P.; Kohn, W. Inhomogeneous Electron Gas. *Phys. Rev.* **1964**, *136* (3B), B864−B871.
(37) Kresse, G.; Joubert, D. From ultrasoft pseudopotentials to the projector augmented-wave method. *Phys. Rev. B* **1999**, *59*, 1758−1775.
(38) Perdew, J. P.; Burke, K.; Ernzerhof, M. Generalized Gradient Approximation Made Simple. *Phys. Rev. Lett.* **1996**, *77*, 3865−3868.
(39) Yang, W.; Xiao, X.; Li, M.; Hu, J.; Xiao, X.; Tong, G.; Chen, J.; He, Y. Conjugated Ditertiary Ammonium Templated (100)-Oriented 2D Perovskite with Efficient Broad-Band Emission. *Chem. Mater.* **2021**, *33* (12), 4456−4464.
(40) Robinson, K.; Gibbs, G. V.; Ribbe, P. H. *Science* **1971**, *172*, 567−570.
(41) Liu, Y.; Wang, A.; Wang, C.; Li, Z.; Hu, G.; Sui, S.; She, J.; Meng, W.; Li, W.; Deng, Z. Alkylamine screening and zinc doping of highly luminescent 2D tin-halide perovskites for LED lighting. *Mater. Adv.* **2021**, *2* (4), 1320−1327.
(42) Li, G.; Fu, C.; Shi, W.; Jiao, L.; Wu, J.; Yang, Q.; Saha, R.; Kamminga, M. E.; Srivastava, A. K.; Liu, E.; Yazdani, A. N.; Kumar, N.; Zhang, J.; Blake, G. R.; Liu, X.; Fahlman, M.; Wirth, S.; Auffermann, G.; Gooth, J.; Parkin, S.; Madhavan, V.; Feng, X.; Sun, Y.; Felser, C. Dirac Nodal Arc Semimetal $PtSn_4$: An Ideal Platform for Understanding Surface Properties and Catalysis for Hydrogen Evolution. *Angew. Chem., Int. Ed.* **2019**, *58* (37), 13107−13112.
(43) Urbach, F. The Long-Wavelength Edge of Photographic Sensitivity and of the Electronic Absorption of Solids. *Phys. Rev.* **1953**, *92* (5), 1324−1324.
(44) Tang, H.; Lévy, F.; Berger, H.; Schmid, P. E. Urbach tail of anataseTiO_2. *Phys. Rev. B* **1995**, *52* (11), 7771−7774.
(45) Tauc, J. Optical properties and electronic structure of amorphous Ge and Si. *Mater. Res. Bull.* **1968**, *3*, 37−46.
(46) Zhang, X.; Wang, C.; Zhang, Y.; Zhang, X.; Wang, S.; Lu, M.; Cui, H.; Kershaw, S. V.; Yu, W. W.; Rogach, A. L. Bright Orange Electroluminescence from Lead-Free Two-Dimensional Perovskites. *ACS. Energy. Lett.* **2019**, *4* (1), 242−248.
(47) Lermer, C.; Birkhold, S. T.; Moudrakovski, I. L.; Mayer, P.; Schoop, L. M.; Schmidt-Mende, L.; Lotsch, B. V. Toward Fluorinated Spacers for MAPI-Derived Hybrid Perovskites: Synthesis, Characterization, and Phase Transitions of $(FC_2H_4NH_3)_2PbCl_4$. *Chem. Mater.* **2016**, *28* (18), 6560−6566.

https://doi.org/10.1021/acsomega.4c01835
ACS Omega 2024, 9, 22352−22359